Earth Surface Processes and Landforms
Earth Surf. Process. Landforms **25**, 437–453 (2000)

EQUILIBRATION OF SALTATION

PETER-JOST SPIES AND IAN K. McEWAN*
Department of Engineering, University of Aberdeen, Aberdeen, AB24 2UE, UK

Received 12 January 1998; Revised 2 July 1999; Accepted 16 August 1999

ABSTRACT

A two-dimensional numerical model of the saltation process was developed on a parallel computer in order to investigate the temporal behaviour of transport rate as well as its downwind distribution. Results show that the effects of unsteady flow on the transportation of particulates (sediment) have to be considered in two spatial dimensions *(x, y)*.

Transport rate *Q(x, t)* appears in the transport equation for mass *M(x, t)*:

$$\frac{1}{A}\frac{\partial M}{\partial t} = -\frac{\partial Q}{\partial x} + S$$

where $A = \Delta x W$ denotes unit area composed of unit streamwise length Δx and width *W*. *S(x, t)* (units kg m^{-2} s^{-1}) stands for the balance over the splash process. A transport equation for transport rate itself

$$\frac{\partial Q}{\partial t} = -U_c\frac{\partial Q}{\partial x} - Q\frac{\partial U_c}{\partial x} + \frac{\partial}{\partial t}(\Delta x S)$$

is suggested with U_c (x, t) a mean particle velocity at location x as the characteristic velocity of the grain cloud.

For a steadily blowing wind over a 50 m long sediment bed it was found that downwind changes in Q cease after roughly 10–40 m, depending on the strength of the wind. The onset of stationarity ($\partial/\partial t = 0$) was found to be a function of the friction velocity and location. The local equilibrium between transport rate and wind was obtained at different times for different downstream locations. Two time scales were found. One fast response (in the order of 1) to incipient wind and a longer time for equilibrium to be reached throughout the simulation length. Transport rate also has different equilibrium values at different locations.

A series of numerical experiments was conducted to determine a propagation speed of the grain cloud. It was found that this velocity relates linearly to friction velocity. Copyright © 2000 John Wiley & Sons, Ltd.

KEY WORDS: Saltation; transport rate; friction velocity; unsteady flow

INTRODUCTION

Previous investigations into the behaviour of the saltation cloud were largely restricted to steady, one-dimensional winds. The goal is to relate the sand transport rate to some information about the strength of the wind, and it is still uncertain what functional form that dependency should take. Most existing formulae relate Q to the third power on the boundary layer's friction velocity u_*.

The interaction of the sand cloud with the wind was investigated in models by Ungar and Haff (1987), Werner (1988, 1990), Anderson and Haff (1991) and McEwan and Willetts (1993). A common feature of these models is their one-dimensionality, i.e. the assumption of fully developed flow. Although simulation of the temporal development of the grain cloud was attempted in the models by Anderson and Haff and McEwan, these algorithms use time as an iterative basis to arrive at the equilibrium described by the boundary

* Correspondence to: Dr I. McEwan, Department of Engineering, University of Aberdeen, Fraser Noble Building, Kings' College, Aberdeen, AB24 3UE, UK. E-mail: i.mcewan@aberdeen.ac.uk
Contract/grant sponsor: Natural Environment Research Council; contract/grant number: GR3/8413

conditions. This is somewhat analogous to a wind tunnel experiment in which wind of a fixed steady flow rate passes over a mobile sand bed, neglecting effects of the developing boundary layer. The downwind coordinate is then identified with time.

What is the spatial development of the grain cloud in steady and unsteady winds? Naturally occurring wind is never truly one-dimensional. The near-surface flow over a strip of beach for example is three-dimensional owing to surface uneveness. Disregarding topographic effects, boundary layer flow is still two-dimensional owing to its development in flow direction.

Experimental observations of the temporal and downwind behaviour of the salation cloud were made by Bagnold (1936), who gave a qualitative description of transient effects and the spatial distribution of Q in his wind tunnel experiments. Shao and Raupach (1992) measured the streamwise distribution of transport rate for fixed times, $Q_t(x)$, in their experiments. Subsequently, researchers using wind tunnels observed and accounted for the same phenomena of time and length needed to reach a steady state in their investigation (Owen and Gillette, 1985).

In order to resolve the temporal as well as the spatial changes of the grain cloud the flow has to be simulated in two dimensions and time. The assumption of uniform flow no longer applies, because of the possible difference between the wind velocity and the grain cloud's propagation speed.

An important aspect about equilibration in natural flows is the influence of gusts, i.e. turbulence, on the grain advection. In the neutral atmospheric surface layer the turbulent velocity fluctuations exhibit frequencies of 1 to 10 cycles per minute (Kaimal *et al.*, 1972; Wyngaard, 1992). These gusts have long been suspected to influence sand transport at least through aerodynamic dislodgement sweeps (Malina, 1941; Kalinske, 1943; Anderson *et al.*, 1991; Williams *et al.*, 1994). The characteristic eddy velocity 'felt' near the ground can be as much as 83 per cent of the outer flow velocity U_∞ (Cantwell, 1981). The question arises whether u_* is the correct choice for the wind information, since it is, like the mean velocity, an average value of the turbulent flow. (Detailed information about the turbulence was lost in obtaining u_*.) Fortunately, other velocities in the near-wall flow will scale with the friction velocity which is the only velocity scale in the lower part of the boundary layer (Tennekes and Lumley, 1972). Velocities of interest with respect to turbulence influence on the transport of particles are the fluctuating velocities in the horizontal and vertical, and these can be expressed as a function of u_*.

As for the influence of turbulence on transport rate, Horikawa *et al.* (1984) investigated sand transport on a beach and incorporated wind fluctuations into their formula. Kadib (1965) used a statistical model to simulate the grain entrainment due to wind fluctuations; his formula was developed from field observations. Butterfield (1991) investigated the response time of the grain cloud to rapidly varying wind in a wind tunnel.

This report presents a two-dimensional numerical model of the grain–wind interactive process, which was developed out of the existing one-dimensional model by McEwan (McEwan and Willetts, 1993). The computer program was rewritten to simulate behaviour of the flow and the grain cloud in two spatial dimensions (downwind and height) and time. The effects of turbulence were simulated via random fluctuations in the entrainment of particles.

THE NUMERICAL MODEL

The numerical model is based on three modules: the calculation of the mean wind speed; the calculation of the grain trajectories; and a statistical splash function for the grain–bed collision simulation. The latter was developed by McEwan (1991) using experimental data from Willetts and Rice (1985). The model is described in McEwan and Willetts (1993). For the grain trajectory calculation a first-order accurate Euler scheme with self-adjusting integration step sizes was used (Young and Gregory, 1972).

The calculation of the two-dimensional wind velocity field, $\vec{U} = \vec{U}(\vec{x}, t), \vec{x} = (x, y)^T$, is realized using a fully implicit control volume method on a single grid as described in detail in Hirsch (1988), for example. The physical geometry of 50 m height and 50 m length is mapped onto a computational domain of 100×40 control volumes which expands logarithmically in the vertical.

A mixing length model is employed to calculate the effective viscosity:

$$\tau = \left(\mu + \rho l^2 \left|\frac{\partial U}{\partial y}\right|\right) \frac{\partial U}{\partial y} \tag{1}$$

where μ denotes the absolute viscosity, l denotes the mixing length and $\rho = 1{\cdot}22$ kg m^{-3} is the fluid density. Although strictly speaking, the mixing length model is applicable to flows with only one length scale (Tennekes and Lumley, 1972). it has been successfully used in most models of the saltation layer.

Simulation of the grain cloud

The determination of the particle forces on the wind (two-way coupling) is accomplished by solving the equation of motion:

$$\dot{\vec{x}} = \vec{g} + \frac{3}{4} C_D(Re_p) \frac{\rho}{\rho_p} \frac{1}{d_p} \|\vec{U} - \vec{u}\|(\vec{U} - \vec{u}) \tag{2}$$

where x is the particle acceleration in vector form, g = 9·81 m s^{-2} is acceleration due to gravity $\rho_p = 2650$ kg m^{-3} is the grain density, d_p is particle diameter, C_D is the drag coefficient, u is the particle velocity in vector form and Re_p is the particle Reynolds number in x and y.

The aerodynamic particle entrainment was written as an excess shear stress rule (McEwan, 1991), i.e. neglecting lift and spin of particles. If the fluid bed shear stress τ_s exceeds a certain threshold value τ_t, sand grains are introduced into the flow by giving them a lift-off velocity and a uniformly distributed x-location. The grain diameter is also chosen randomly from a range of available sizes.

The number of grains N_e generated per time step and bed area is determined by:

$$N_e = [\Xi A \Delta t(\tau_s - \tau_t)] \tag{3}$$

where A is the bed area (bed length L times bed width W). The factor (units Ns^{-1} = s m^{-1} kg^{-1}) is availability of sand grains. It can be used to simulate for example different moisture contents, encrusting or sorting and armouring of the sediment bed.Nickling (1988) gives experimental values for L, i.e. counts per unit width and unit time. In these simulations a value of $\Xi = 10^8$ Ns^{-1} was applied which reflects the experiments of Nickling.

The product $A\ \Delta t$ determines only the number of aerodynamically entrained grains. Whereas the value of Δt cannot be chosen freely (Spies, 1996), the size of the bed area can be used to determine the number of grains entrained and hence the computational load as well as the statistical accuracy of the computation. To account for situations in which the product $A\ \Delta t$ is too small, yet the shear stress difference is large enough for entrainment, a Poisson process is started to launch particles (Kloeden and Platen, 1992).

Parallel computer code

In order to accelerate the massive grain-cloud calculations the program was coded as a Master/Slaves topology and ported to a Parsytec Power Xplorer parallel computer with 12 processors (Spies, 1996).

MASS BALANCE EQUATIONS

If viewed by a stationary observer the flow and the sand cloud can be described in a Eulerian manner. Figure 1 shows a control volume of streamwise length Δx, width W and height H. The temporal changes of total particle mass $M = \sum_{i=1}^{N} m_i$within the control volume, $\partial M/\partial t$, equals the sum of incoming flow rate,$\dot{m}_{\text{in}}$, less the outgoing rate,$\dot{m}_{\text{ex}} + \dot{m}_{\text{in}} + \Delta x \partial \dot{m}/\partial x$, plus a term S (units kg m^{-2} s^{-1}) that represents the balance of the splash process, expressed as a flow rate $\dot{m}_s = \Delta x W S$. The splash balance is $S = E + B + D$, where the aerodynamically dislodged mass is denoted by E, B is the mass due to ejected, or 'born', grains and $D < 0$

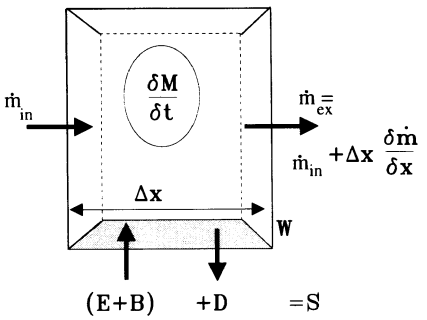

Figure 1. Mass balance for downwind section Δx

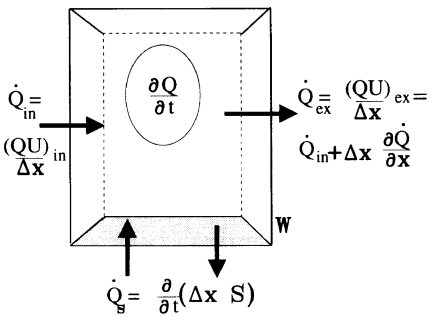

Figure 2. Transport rate balance for a section Δx

stands for the mass of 'dead' impactors (no rebound). Hence:

$$\frac{\partial M}{\partial t} = \dot{m}_{\text{in}} - \left(\dot{m}_{\text{in}} + \Delta x \frac{\partial \dot{m}}{\partial x}\right) + WS\Delta x = -\Delta x \frac{\partial}{\partial x}(WQ) + WS\Delta x \tag{4}$$

where $Q = qH = \dot{m}/W = \dot{m}/AH$ was used for the incoming and outgoing rates. The balance can then be written as:

$$\frac{1}{\Delta x W}\frac{\partial M}{\partial t} = -\frac{\partial Q}{\partial x} + S \tag{5}$$

A similar equation is obtained for transport rate itself (see Figure 2). Incoming and outgoing fluxes of Q are $(U_c Q)_{\text{in}}/\Delta x$ and $(U_c Q)_{\text{ex}}/\Delta x$, respectively, if U_c is a characteristic velocity of the grain cloud. This propagation speed, or celerity, of the grain cloud is now identified with the mean particle velocity at a certain location x:

$$U_c \overset{\text{def}}{=} \frac{1}{N_x}\sum_{i}^{N_x} u_{p,i} \tag{6}$$

The rate of change of Q within a control section Δx is therefore:

$$\frac{\partial Q}{\partial t} = -\Delta x \frac{\partial}{\partial x}\left(\frac{U_c Q}{\Delta x}\right) + \frac{\partial}{\partial t}(\Delta x S) = -\frac{\partial}{\partial x}(U_c Q) + \Delta x \frac{\partial S}{\partial t} \tag{7}$$

And since $\partial U_c/\partial x$ is not necessarily zero:

$$\frac{\partial Q}{\partial t} = -U_c \frac{\partial Q}{\partial x} - Q \frac{\partial U_c}{\partial x} + \Delta x \frac{\partial S}{\partial t} \tag{8}$$

The first term on the right-hand side of Equation 8 looks like a convection term. But since for a fixed U_c the transport rate will vary only because of variations in mass flow rate, it is now suggested that this term describes the concentration gradient and hence the flux potential for transported mass. This notion is supported by the appearance of $-\partial Q/\partial x$ in Equation 5.

The second term reflects differences in the grains' mean speed along the flow direction. These will certainly stem from the inhomogeneity of the developing boundary layer. But in nature, terrain irregularities will have a major effect on this term. The last term in Equation 8 is the temporal change in the bed response. In reality this will be caused mainly by ripple formation, sorting and other effects due to the bed's microtopography.

With the characteristic velocity U_c chosen here as a cloud's celerity which is a quantity of the particle assembly, no direct link to the wind speed is established yet. We present an attempt to make this link in the concluding section.

SIMULATION RESULTS

Steady wind

Figure 3 shows the space–time development of transport rate, $Q(x, t)$, for an effective friction velocity of $u_{*,\mathrm{eff}} = 1{\cdot}0\ \mathrm{m\ s^{-1}}$. (The effective friction velocity is the friction velocity during sediment transport well above the sediment cloud and is larger than the initial, sediment-free friction velocity.) The contour map for Q is presented in Figure 4.

The transport rate shows a strong growth in the first 10 m of the simulation. Two effects are responsible for this. On the one hand bed shear stresses are highest at the upwind end of the simulation, as is the case in nature, where the boundary layer is starting to develop. On the other hand the fluid flow has yet to feel the full effects of the momentum exchange with the particulate phase. This last behaviour has already been successfully simulated with one-dimensional models.

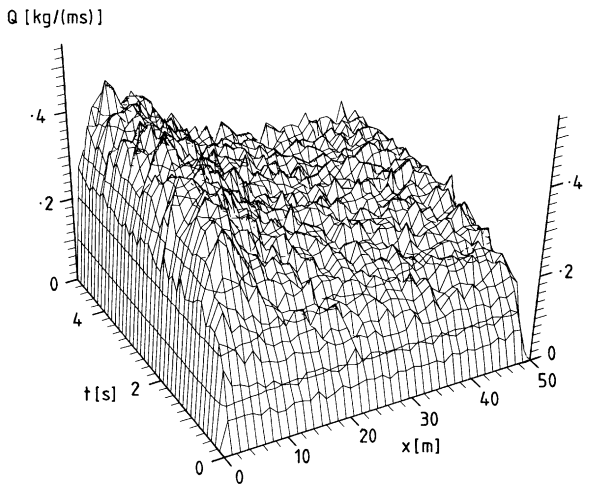

Figure 3. Transport rate development for 5 s along a sediment bed of 50 m. The initial friction velocity was $U_* = 0{\cdot}6\ \mathrm{m\ s^{-1}}$; $U_{*,\mathrm{eff}} = 1{\cdot}0\ \mathrm{m\ s^{-1}}$

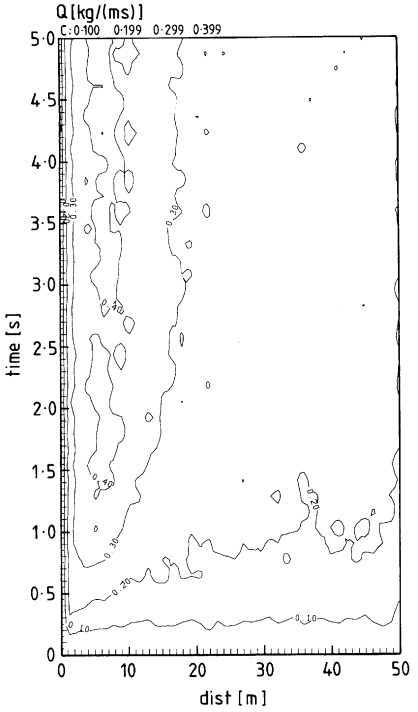

Figure 4. Contour plot of transport rate development. Specifications as for Figure 3

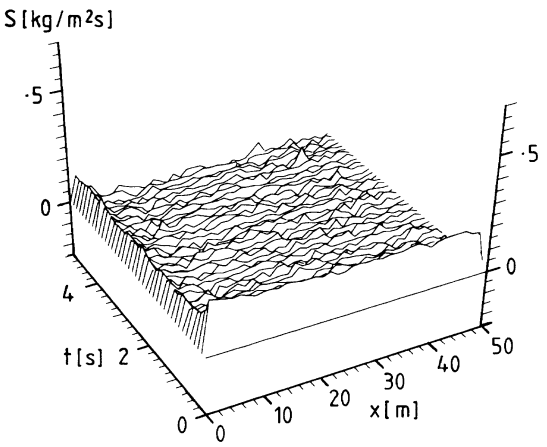

Figure 5. Development of the splash process S for $U_{*,\,\mathrm{eff}} = 1{\cdot}0$ m s^{-1}

Stationarity ($\partial/\partial t = 0$) at any given x-location can be seen in the contour plots as lines parallel to the time axis. After roughly 2 s Q reaches its final stationary value (here of c. 0·4 kg m^{-1} s^{-1}) in the inflow section ($x \lesssim 15$ m). However, further downwind stationarity is not reached until roughly $t = 3$ s at $x \gtrsim 20$ m, where $Q \approx 0{\cdot}2$ kg m^{-1} s^{-1}. This 'plateau' is the equilibrium value. The wind velocity in this area is immediately affected by the momentum extraction upwind and therefore very quickly decelerated. The wind has only the capacity to sustain the sand transport coming from upwind but not enough momentum to further increase Q. Any losses to the grain cloud happen further upwind, so that Q is indeed stationary in this region.

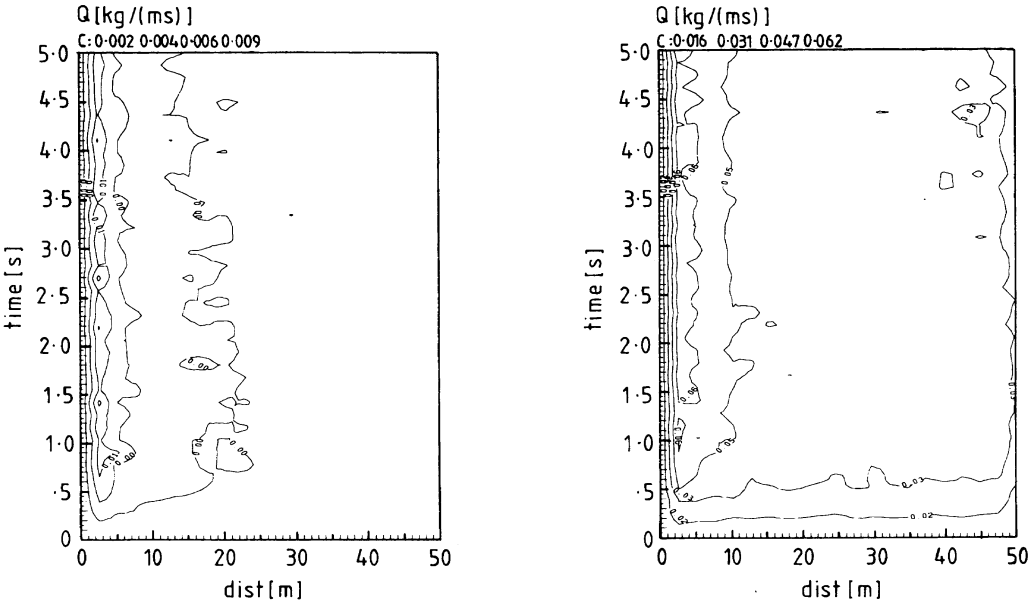

Figure 6. Development of Q for a flow of $U_{*,\,\mathrm{eff}} = 0{\cdot}30$ m s^{-1} (left) and $U_{*,\,\mathrm{eff}} = 0{\cdot}48$ m s^{-1} (right)

The notion of a purely convected grain cloud downwind of roughly 20 m is supported by the x–t graph for the splash balance S in Figure 5. For larger x and t there is no net flux through the bed ($S \approx 0$). Hence the grain cloud cannot be changing. In addition, the large rims on the axes should be noted. These are due to the strong aerodynamic dislodgement at the beginning and near the upwind edge.

The contour plots for the lowest friction velocities tested, $u_{*,\,\mathrm{eff}} = 0{\cdot}3$ and $u_{*,\,\mathrm{eff}} = 0{\cdot}48$ m s^{-1}, show two time scales (Figure 6). In these graphs the first 1·5 s are the principal development of transport rate along the bed. A length of $L_e \approx 20$ m for $u_{*,\,\mathrm{eff}} = 0{\cdot}30$ m s^{-1} ($L_e \approx 50$ m for $u_{*,\,\mathrm{eff}} = 0{\cdot}48$ m s^{-1}) before levelling out to a lower value is associated with this time. After roughly 2 s transport rate between 10–20 m begins to fall. The equilibrium length L_e begins to recede, a process that has not ended after the total simulation time of 5 s. For $u_{*,\,\mathrm{eff}} = 0{\cdot}48$ m s^{-1} this behaviour is best seen in the recess of the contour line near the downwind end. In this test case equilibrium (stationarity) had not been reached either. Reflecting on the results of the one-dimensional simulation, we recall that in weak winds the second time scale after overshooting is longer than in stronger winds. The adjustment of wind velocity to the sand-borne roughness, described in. Panofsky (1974) for example, takes in the order of tens of seconds. This must be viewed as an overall feature of a sand–wind system as it appears in the one- as well as the two-dimensional simulations.

In the graphs for the aerodynamic entrainment (Figure 7) and the splash balance (Figure 8, left) the temporal characteristics of this flow become apparent. A strong initial aerodynamic dislodgement at the beginning and in the inlet section generates the grain cloud that subsequently diminishes for downwind locations $x \gtrsim 5$ m. Far downwind, $x \gtrsim 20$ m, the splash flux S is zero. Between 10 and 15 m at later times a slight trench ($S < 0$) can be made out. A negative splash balance is expected in this area since the decreased wind velocity cannot carry the superfluous amount of sand that was entrained upstream. The graph for $\partial M/\partial t$ (Figure 8, right) shows the large negative value near the upwind edge, which is explained by a large $\partial Q/\partial x$ in the first control volume. After this 'trench' in the x–t graph, a 'ridge' can be seen which flattens out towards larger times. This feature reflects the ongoing changes in Q mentioned above.

Advection

In order to evaluate the propagation speed of the grain cloud mentioned above, cloud advections at different wind speeds were simulated. A grain cloud was generated by allowing aerodynamic entrainment in a

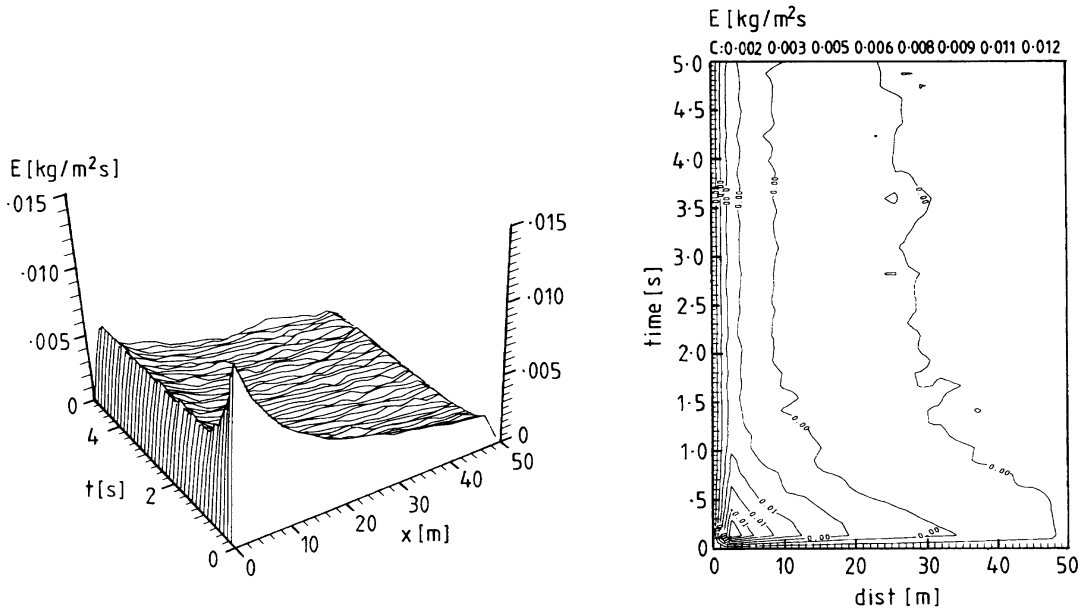

Figure 7. Development of E for a two-dimensional flow of $U_{*,\,\mathrm{eff}} = 0{\cdot}30$ m s^{-1}

limited section of the bed length ($x \leq 10$ m) and for a limited time only ($t < 0{\cdot}1$ s). This cloud was then left to be advected downwind with bed exchanges still being allowed, but no aerodynamic dislodgement ($\Xi = 0$).

Figures 9 to 13 show the $Q(x, t)$ graphs and contour plots for $u_* = 0{\cdot}4$, $0{\cdot}6$, $0{\cdot}8$, $1{\cdot}0$ and $1{\cdot}2$ m s^{-1}. (Since the transport of sediment is limited to the extent of the cloud, the wind is largely unaltered. A distinction between an effective and an initial friction velocity is not necessary.)

For $u_* = 0{\cdot}4$ m s^{-1} the cloud diminishes during its journey; the splash process is a net loss – the wind is not strong enough to sustain high particle velocities. Since only aerodynamic entrainment is excluded from these simulations and the friction velocity is larger than the impact threshold, this means that for a weak wind the aerodynamic dislodgement is necessary to sustain Q for a steady-state transport. The graph also suggests that the front of the cloud is propagating more slowly than the back. This is surprising, since it is expected that no matter how strongly the wind blows, a sorting of grains by speed would be portrayed in $Q(x,t)$. The reason for a slower front must be that the sand transport is made up mainly of slow ejecta that 'die' on the first impact. The wind velocity is larger upwind of the cloud; here the grains are faster than in the front of the cloud. For $u_* = 0{\cdot}6$ m s^{-1} Q stays at a constant level throughout the journey; the splash flux must be zero, or $B + E = -D$.

At the higher friction velocities ($u_* \geq 0{\cdot}8$ m s^{-1}) the sand transport rate increases steadily. The splash process is in itself enough to raise Q. The theoretical upper limit of Q is determined by the wind speed which cannot be exceeded by the particles. Further, the back of the grain cloud propagates more slowly and is steeper than the front. A possible explanation for this is that there is no limitation of the particle velocities towards greater velocities. But at the low-speed end of particle speeds there is a natural cut-off: slow-moving grains are less likely to rebound.

Entrainment flurries

The standard deviation of longitudinal wind velocity fluctuations, i.e. gusts, can be estimated with, for example, $\sigma_u = 2{\cdot}5u_* = 2{\cdot}5\sqrt{\tau/\rho}$ (Lumley and Panofsky, 1964). For the presented test case of $u_{*,\mathrm{init}} = 0{\cdot}4$ m s^{-1} ($u_* = u_{*,\mathrm{eff}} \approx 0{\cdot}48$ m s^{-1}) this amounts to $1{\cdot}2$ m s^{-1}. In the following simulations a maximum value of

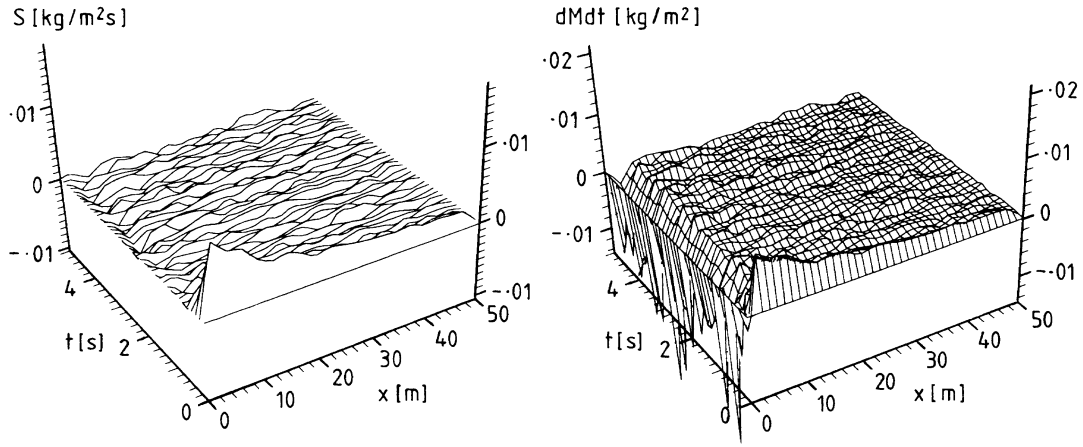

Figure 8. Development of the splash process S (left) and $\partial M/\partial t$ (right) for a two-dimensional flow of $U_{*,\,\mathrm{eff}} = 0{\cdot}30$ m s^{-1}

$\tilde{u} = U + 2\sigma_u$ was assumed. The maximum shear stress excursion is then estimated as:

$$\tau_{\max} \approx \rho u_*^2 + \rho(2 \times 2 \cdot 5u_*)^2 = \rho u_*^2(1 + 25) \tag{9}$$

which is 26 times higher than the average. A very conservative estimate of $\tau_{\max} = 11\rho u_*^2$ was then used to evaluate the instantaneous entrainment factor from the mean and the normal-distributed fluctuations;

$$\bar{\xi}(x) = \Xi + \xi(x), \quad \xi = \mathrm{N}(\Xi, \sigma_\xi) \tag{10}$$

where the standard deviation for ξ was estimated as;

$$\sigma_\xi \approx \frac{\sigma_\tau \Xi}{\rho u_*^2} = 5\Xi \tag{11}$$

Equation 11 means that for a maximum gust of $\xi = \Xi + 2\sigma_\xi$, 11 times as many grains as for a steady wind will be entrained.

Since the duration of a gust is inversely proportional to its strength (Kristensen *et al.*, 1991) the 'flurry' duration T_ξ was evaluated as:

$$T_\xi = \frac{2\sigma_\xi}{|\xi|} T_{\max} \tag{12}$$

from the arbitrarily set duration of the strongest gusts, $T_{\max} = 0{\cdot}5$ s.

The sequence of excursions is Poisson-distributed if they are statistically independent events (Kristensen *et al.*, 1991). Instead of using a Poisson process new flurries were allowed after the previous ones had finished, choosing randomly between one or two gusts along the simulation length. Following Kristensen *et al.* (1991) a probability of $P(n = 1) = 0{\cdot}37$ for one gust and $P(n = 2) = 0{\cdot}26$ for two was used. The velocity fluctuations then occurred as a succession of ξ-variations described by Equation 10.

Figure 14 shows the aerodynamic entrainment flux $E(x,t)$ for a test case with $u_* = u_{*,\mathrm{eff}} \approx 0{\cdot}48$ m s^{-1}. Apart from the expected 'rims' near the inlet and the x-axis, the simulated flurries can be seen as peaks in the x–t-graph and as spots in the contour plot.

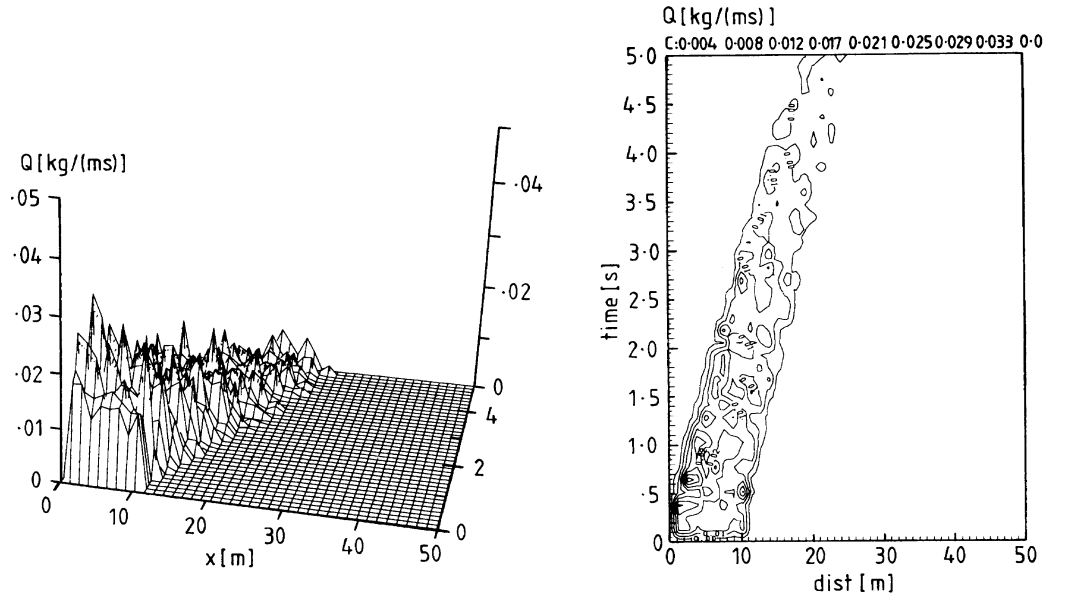

Figure 9. Convection of the grain cloud. $U_{*,\,\mathrm{eff}} = 0{\cdot}40\ \mathrm{m\ s^{-1}}$. The cloud diminishes during its journey, the splash process is a net loss. The wind is not strong enough to sustain saltation

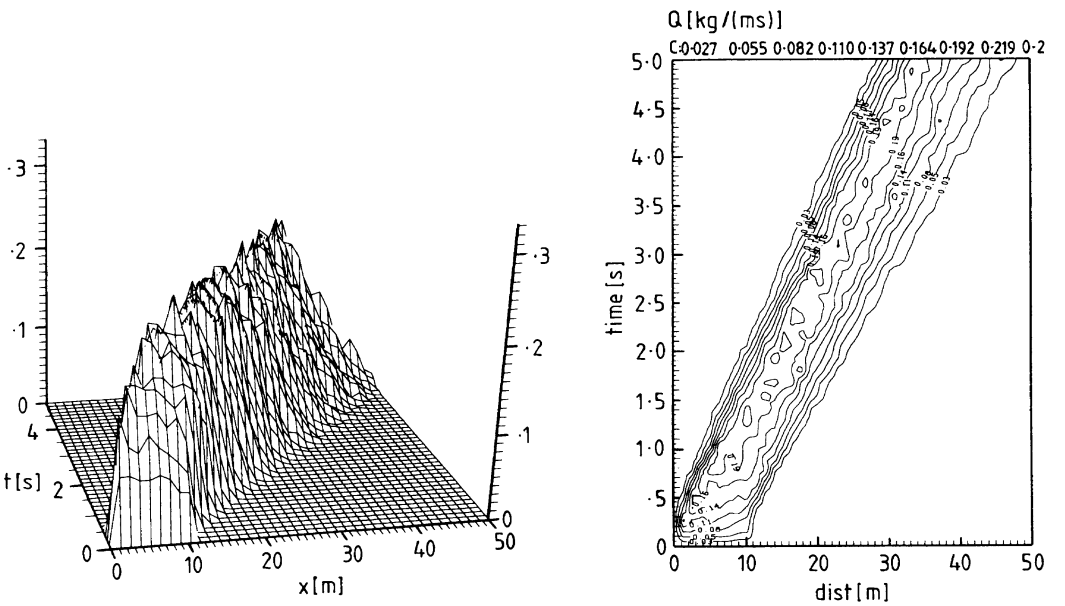

Figure 10. Convection of the grain cloud. $U_{*,\,\mathrm{eff}} = 0{\cdot}60\ \mathrm{m\ s^{-1}}$. The cloud retains its magnitude. $DQ/Dt = 0$

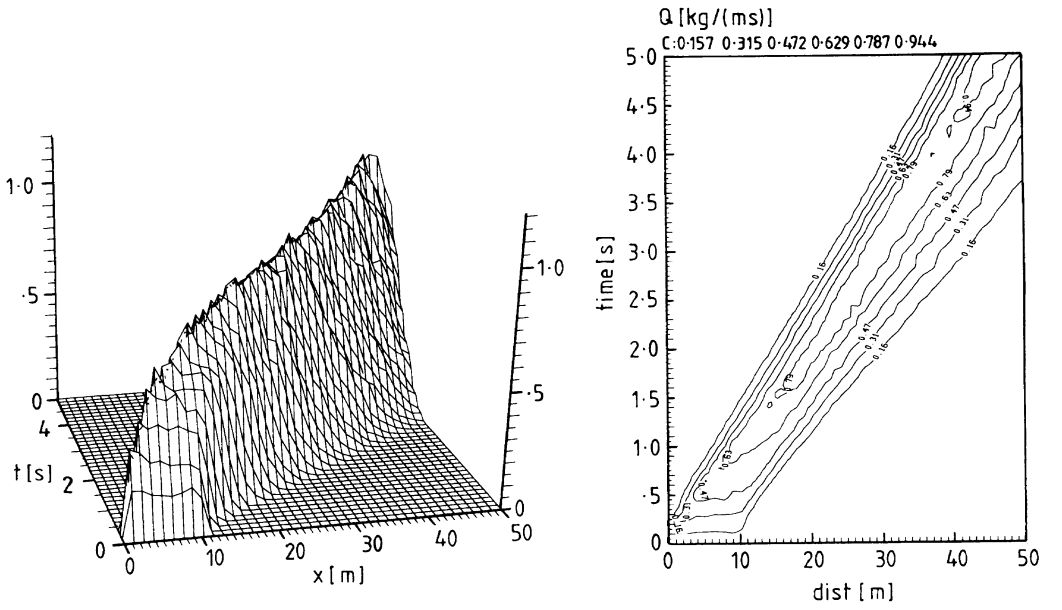

Figure 11. Convection of the grain cloud. $U_{*,\,\mathrm{eff}} = 0{\cdot}80\ \mathrm{m\,s^{-1}}$. The grain cloud is growing during the journey, the splash process is a net gain

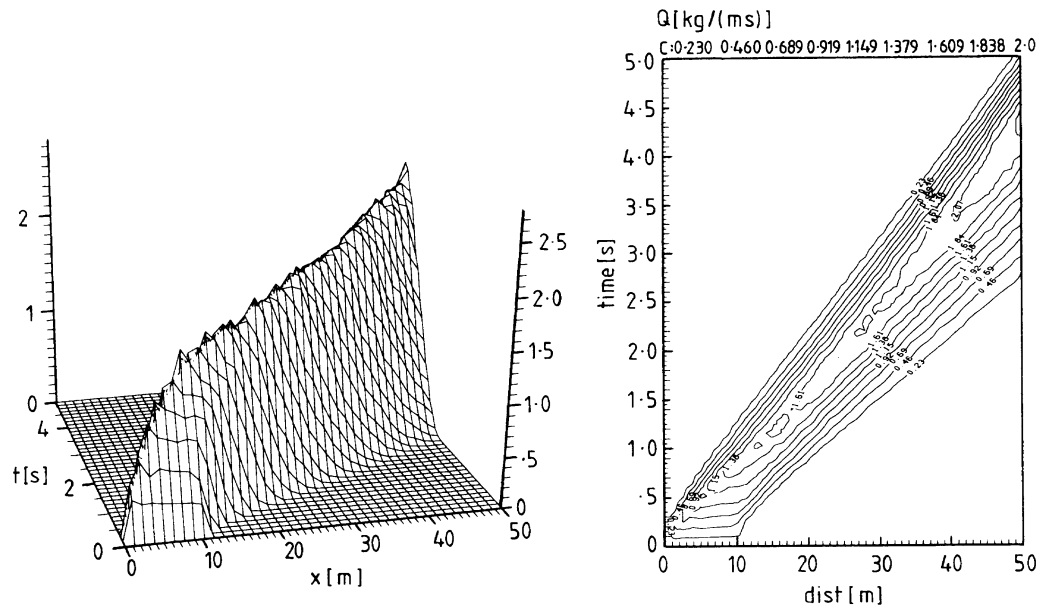

Figure 12. Convection of the grain cloud. $U_{*,\,\mathrm{eff}} = 1\ \mathrm{m\,s^{-1}}$. Strong growth of the grain cloud – avalanching

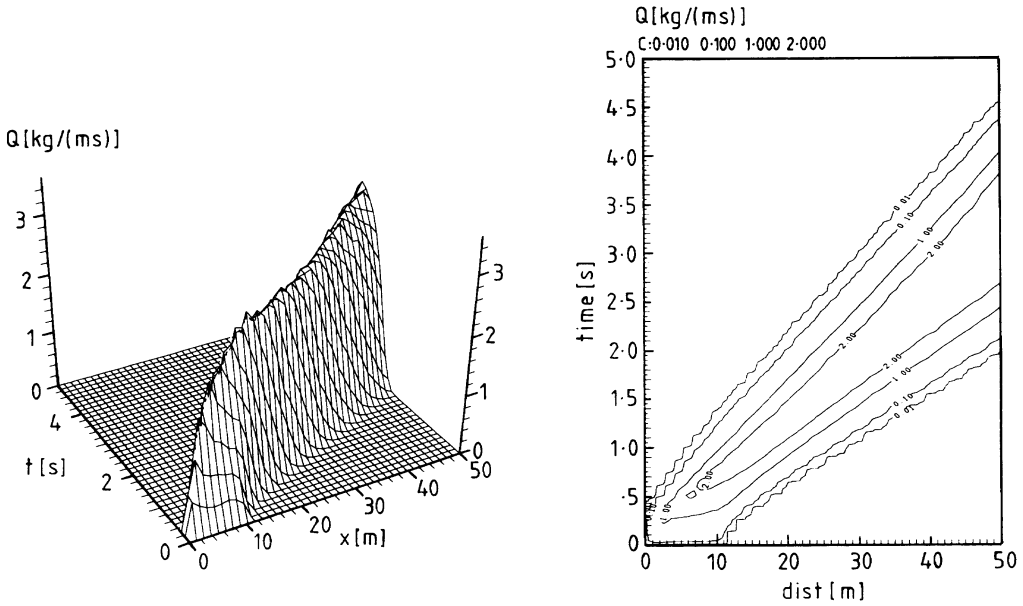

Figure 13. Convection of the grain cloud. $U_{*,\,\mathrm{eff}} = 1{\cdot}2\ \mathrm{m\ s^{-1}}$

Naturally, the transport rate (Figures 15 and 16) is occasionally larger than the average value (compare with Table I). As a whole Q is raised in wide areas for a substantial time above the steady-wind value. Depending on gust duration and strength, the transport rate will be affected immediately downwind of the ξ-spot. It must be pointed out here that the wind speed is not raised during a simulated 'gust'. Hence the advection of a gust-borne peak in Q is still underpredicted by the program. One reason why numerical models underpredict sand transport rates typically occurring in nature could be a missing model of turbulence influence.

CONCLUSIONS

The numerical model presented is capable of simulating temporal variations in wind speed in two spatial dimensions.

Transport equations for grain mass and transport rate itself have been presented. Previous attempts to derive a transport equation for Q did not start with a balance analysis over a control section of the flow and tried to relate the substantive derivative of Q

$$\frac{DQ}{Dt} = \frac{\partial Q}{\partial t} + U\frac{\partial Q}{\partial x}$$

to the bed response. This approach is valid only if U does not change. Because of the spatial distribution of the grain cloud, this latter assumption cannot be guaranteed. It is now understood that the first two terms on the

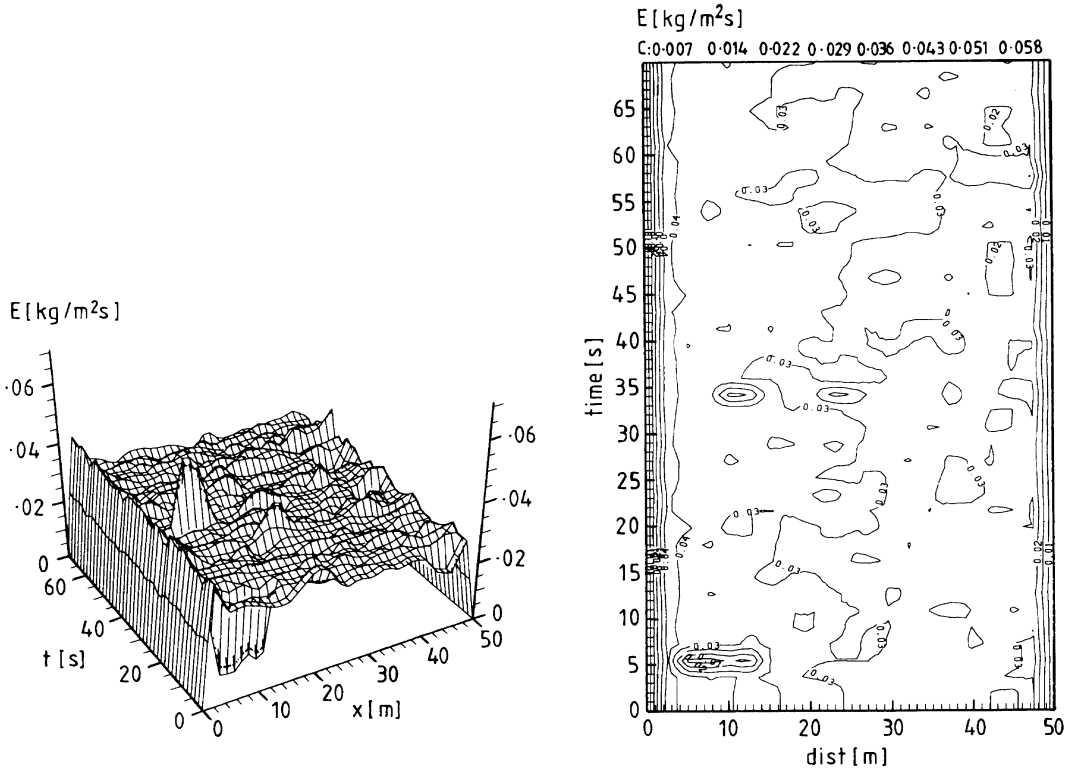

Figure 14. Fluctuations in the entrainment flux E for average wind speed of $U_{*,\,\mathrm{eff}} = 0{\cdot}48\ \mathrm{m\,s^{-1}}$. Individual spots of increased entrainment flux are distinguishable. Simulation of 70 s

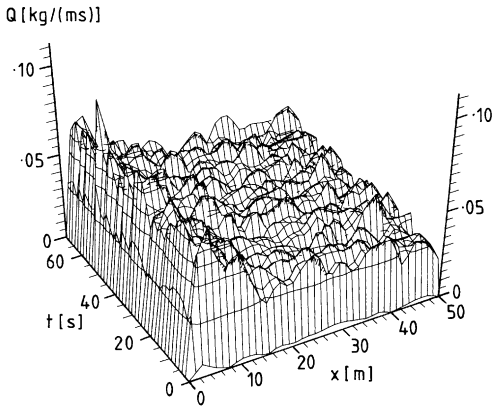

Figure 15. Transport rate with simulated gusts for $U_{*,\,\mathrm{eff}} = 0{\cdot}48\ \mathrm{m\,s^{-1}}$. A slightly higher value for Q is obtained than for the same wind speed without fluctuations

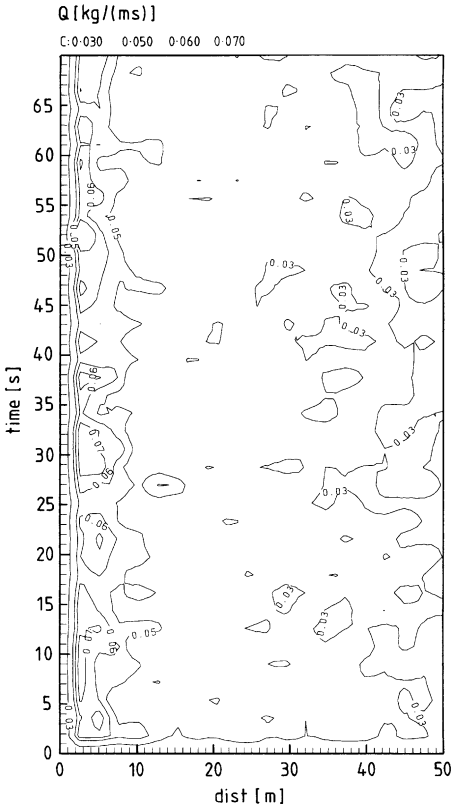

Figure 16. Contour plot of $Q(x,t)$ for the 'flurry' test case. Simulation of 70 s

Table I. Summary of steady two-dimensional results

$u_{*,\,\mathrm{init}}$ (m s^{-1})	$u_{*,\,\mathrm{eff}}$ (m s^{-1})	$Q_{\max}$ (kg m^{-1} s^{-1})	L_o (m)	t_e (s)	L_e (m)	Q_e (kg m^{-1} s^{-1})
0·3	0·30	0·01	5	1·0	< 20	0·002
0·4	0·48	0·05	10	2·0	20	0·03
0·5	0·60	0·19	15	3·0	40	0·09
0·6	1·00	0·44	20	3·5	50	0·2
0·7	1·15	0·86	30	4·0	> 50	$< 0·4$

$u_{*,\,\mathrm{init}}$, initial friction velocity; $u_{*,\,\mathrm{eff}}$, effective friction velocity; $Q_{\max}$, maximum transport rate; L_o, overshoot length; t_e, time to reach equilibrium over whole length; L_e, length needed to reach equilibrium; Q_e, equilibrium value for transport rate

right-hand side of

$$\frac{\partial Q}{\partial t} = -U_c \frac{\partial Q}{\partial x} - Q \frac{\partial U_c}{\partial x} + \Delta x \frac{\partial S}{\partial t}$$

are of the same order of magnitude. Upstream of the sand bed, i.e. the first 1–2 after the inlet, both terms complement each other to roughly zero ($-U_c \partial Q/\partial x < 0$ and $-Q \partial U_c/\partial x > 0$). The test calculations for

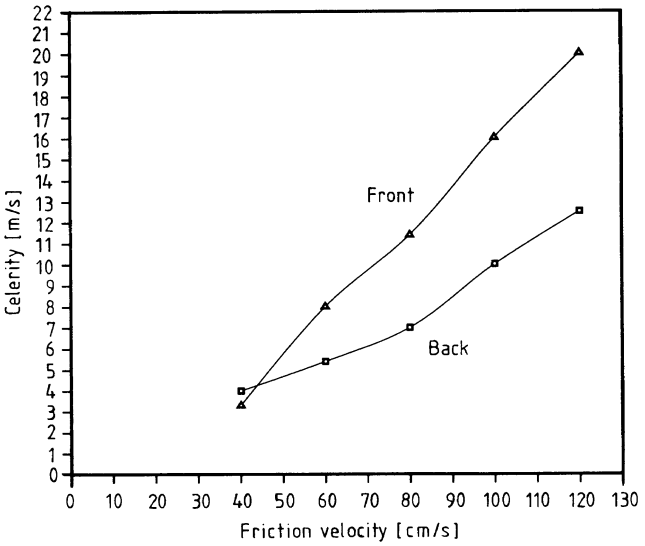

Figure 17. Celerity of the grain cloud; measured at the front and back of the cloud. For the front $C \approx 21{\cdot}25\ U_{*,\,\mathrm{eff}}$; for the back $C \approx 12{\cdot}5\ U_{*,\mathrm{eff}}$

$u_{*,\mathrm{eff}} = 1{\cdot}0$ m s^{-1} show good agreement between the right-hand side of the above equation and the temporal derivative of Q.

Equilibration of the saltation cloud was investigated by simulating a steadily blowing wind. The spatial distribution of Q shows the effect of the developing boundary layer. Downwind locations are affected by the development upstream and different equilibrium values for Q are found at different locations. Simulations results show that transport rate assumes varying equilibrium values at different downwind distances. The time needed to arrive at stationary values depends on the location as well as the average wind speed. Two time scales are predicted by the two-dimensional calculations, as well as by the one-dimensional predictions of previous investigations; a first fast response (1–2 s) of the sand grains to incipient wind, and a second, much longer time for stationarity to be attained throughout the whole model length.

Results for maximum transport rate, $Q_{\max}$, length of overshoot, L_o, time to reach the equilibrium, t_e, length needed for equilibrium, L_e, and the equilibrium value for sand transport, Q_e, are summarized in Table I.

In order to determine the cloud's celerity, pure advection tests were performed with the model. The propagation speed was found to relate linearly to the friction velocity; for the bed response model used here the relation was $C \approx 21u_{*,\mathrm{init}}$. (In these advection tests the propagation speed of the grain cloud was overpredicted because the wind velocity remained unaffected at the front of the cloud). Figure 17 shows the celerity versus u_*. The slope of the curve for 'front' measurements is 21·25; for the 'back' $C \approx 12{\cdot}5\ u_*$.

The characteristic cloud velocity U_c used in the balance equation for Q (Equation 8) is a particle quantity. The celerity 'measurements' presented here cannot be used as information towards U_c since in the advection tests a constant wind was driving the grain cloud. Momentum extraction due to grains was localized within the extent of the grain cloud itself, which means that unaffected strong winds downwind accelerate all active grains near the front of the cloud. This results in the faster propagation and a surging effect at the front. Hence always $C > U_c$, except for the weak wind of $u_* = 0{\cdot}4$ m s^{-1}. (The celerity for $u_* = 0{\cdot}6$ cm s^{-1} is about twice as much as U_c.)

A second possibility to establish a connection between the fluids and the grain velocity could be the wind speed at a suitably chosen height h_c within influence of the saltation layer, so that:

$$\frac{\partial Q}{\partial t} = -\frac{\partial}{\partial x}(U(h_c(u_*))Q) + \Delta x S \tag{13}$$

U_c is linked to the mean wind velocity via the trajectory calculations. A more direct link to the fluid phase is wished for, i.e. a functional dependency like $U_c = f(U(h_c))$, in which h_c stands for a characteristic height of the saltation layer with a wind velocity U affecting the bulk of the grains.

The simulation of turbulence effects on the advection of the grain cloud highlights the fact that sand transport in unsteady winds must be considered in two dimensions. The 'flurry' tests simulate gusty fluctuations in the dislodgement. Deviations from an average entrainment cause the transport rate to vary locally and – through advection – downwind. Predictions should account for these fluctuations if applied to natural flows. Since there are no 'gusts' in wind tunnels (eddy size is too small in relation to particle size), laboratory experiments will underpredict Q. Better answers could be achieved via the simulation of 'gusts' by varying the mean wind speed in the tunnel. Since this affects the whole of the tunnel immediately, it must be ensured that the latter has the length of an eddy.

ACKNOWLEDGEMENTS

The authors acknowledge the financial support of the Natural Environment Research Council of the UK under grant GR3/8413. Graeme Butterfield was a co-investigator on this project and provided much of the stimulus that led to this work. We are grateful to him for this.

REFERENCES

Anderson, R. S.and Haff, P. K. 1991. Wind modification and bed response during saltation of sand in air. In Acta Mechanica Suppl. 1, Barndorff-Nielsen, O. E. and Willetts, B. B. (eds). Springer-Verlag: Berlin; 21–51.

Anderson, R. S., Sørensen, M. and Willetts, B. B. 1991. A review of recent progress in our understanding of aeolian sediment transport. In Acta Mechanica Suppl. 1, Barndorff-Nielsen, O. E. and Willetts, B. B. (eds). Springer-Verlag: Berlin; 1–19.

Bagnold, R. A. 1936. The movement of desert sand. *Royal Society, Proceedings* **A157**: 594–620.

Butterfield, G. R. 1991. Grain transport rates in steady and unsteady turbulent air flows. In Acta Mechanica Suppl. 1, Barndorff-Nielsen, O. E. and Willetts, B. B. (eds). Springer-Verlag: Berlin; 97–122.

Cantwell, B. J. 1981. Organized motion in turbulent flow. *Annual Review of Fluid Mechanics* **13**: 457–515.

Hirsch, C. 1988. Numerical Computation of Internal and External Flows, Vol. 1 Fundamentals of Numerical Discretization. Wiley: Chichester.

Horikawa, K., Hotta, S., Kubota, S. and Katori, S. 1984. Field measurement of blown sand transport rate by trench trap. *Coastal Engineering Japan* **27**: 213–232.

Kadib, A. A. 1965. A Function of Sand Movement by Wind. Technical Report **HEL-2-12**, Institute of Engineering Research. University of California, Berkeley.

Kaimal, J. C., Wyngaard, J. C., Izumi, Y. and Coté, O. R. 1972. Spectral characteristics of surface-layer turbulence. *Quarterly Journal of the Royal Meteorological Society* **98**: 563–589.

Kalinske, A. A. 1943. Turbulence and the transport of sand and silt by wind. *Annals of the New York Academy of Science* **44**: 41–54.

Kloeden, P. E. and Platen, E. 1992. Numerical Solution of Stochastic Equations. Applications in Mathematics, 23. Springer: Berlin.

Kristensen, L., Casanova, M., Courtney, M. S. and Troen, I. 1991. In search of a gust definition. *Boundary-Layer Meteorology* **55**: 91–107.

Lumley, J. L. and Panofsky, H. A. 1964. The Structure of Atmospheric Turbulence. Interscience: London.

Malina, F. J. 1941. Recent development in the dynamics of wind-erosion. *Transaction of the American Geophysical Union* **22**: 262–286.

McEwan, I. K. 1991. The Physics of Sand Transport by Wind. PhD thesis, University of Aberdeen.

McEwan, I. K. and Willetts, B. B. 1993. Adaption of the near-surface wind to the development of sand transport. *Journal of Fluid Mechanics* **252**: 99–115.

Nickling, W. G. 1988. The initiation of particle movement by wind. *Sedimentology* **35**: 499–511.

Owen, P. R. and Gillette, D. 1985. Wind tunnel constraint on saltation. In Proceedings of the International Workshop on the Physics of Blown Sand. Memoirs No. 8. Vol. 2, Department of Theoretical Statistics, Institute of Mathematics, University of Arhus: Denmark; 253–269.

Panofsky, H. A. 1974. The atmospheric boundary layer below 150 meters. *Annual Review of Fluid Mechanics* **16**: 147–177.

Shao, Y. and Raupach, M. R. 1992. The overshoot and equilibration of saltation. *Journal of Geophysical Research* **97**(D18): 20559–20564.

Spies, P. J. 1996. The Transport of Sand in Unsteady Winds. PhD thesis. University of Aberdeen.
Tennekes, H. and Lumley, J. L. 1972. A First Course in Turbulence. MIT Press: Cambridge, Mass.
Ungar, J. E. and Haff, P. K. 1987. Steady state saltation in air. *Sedimentology* **34**: 289–299.
Werner, B. T. 1988. A Steady-state Model of Wind-blown Sand Transport. The Blue and White Reports on the Dynamics of Granular Materials **1**. Research Department, Naval Weapons Center: China Lake, Calif.
Werner, B. T. 1990. A steady-state model of wind-blown sand transport. *Journal of Geology* **98**: 1–17.
Willetts, B. B. and Rice, M. A. 1985. Inter-saltation collisions. In Proceedings of the International Workshop on the Physics of Blown Sand. Memoirs No. 8. Department of Theoretical Statistics, Institute of Mathematics, University of Århus: Denmark; 83–100.
Williams, J. J., Butterfield, G. R. and Clark, D. G. 1994. Aerodynamic entrainment threshold: effects of boundary layer flow conditions. *Sedimentology* **41**: 309–328.
Wyngaard, J. C. 1992. Atmospheric turbulence. *Annual Review of Fluid Mechanics* **24**: 205–233.
Young, D. M. and Gregory, R. T. 1972. A Survey of Numerical Mathematics, Reading, Mass., Addison-Wesley.

